Ultrafast and low-power dynamically tunable plasmon induced transparency in dual ring cavities coupled MDM plasmonic waveguide system

B. WANG[a,b,*], Y. LING[b], Q. ZENG[a], L. XIONG[a], H. LV[a], C. XU[c], J. DU[a], H. YU[a,*]
[a]*School of Physics and Electronic-information Engineering, Hubei Engineering University, Xiaogan 432000, People's Republic of China*
[b]*Wuhan National Laboratory for Optoelectronics, Huazhong University of Science and Technology, Wuhan 430074, People's Republic of China*
[c]*Department of Physics, New Mexico State University, Las Cruces, NM 88001, United States of America*

We theoretically and numerically investigate an ultrafast and low-power dynamically tunable plasmon induced transparency (PIT) in dual ring cavities side-coupled with a metal-dielectric-metal (MDM) plasmonic waveguide system. With dynamically tuning the propagation phase of the plasmonic waveguide, π-phase shift of the transmission spectrum in the PIT system is achieved under excitation of a pump light with an intensity as low as 5.83 MW/cm^2. The group delay is controlled between 0.19 and 0.68 ps. This work provides a simple approach for designing ultrafast and tunable PIT devices and has potential applications in ultrafast optical switching, ultrasensitive sensor and light storage.

(Received December 5, 2018; accepted August 20, 2019)

Keywords: Plasmon induced transparency (PIT), Graphene, Optical Kerr effect, Ring resonators, Plasmonic waveguide

1. Introduction

In electromagnetically induced transparency (EIT), quantum destructive interference among excitation pathways to the upper level in three-level atomic systems has led to a sharp cancellation of absorption in the medium[1, 2], resulting in promising applications, such as nonlinear optical processes, ultrafast switching, and optical data storage owing to the strong dispersion in the transparency windows [3, 4]. However, the practical applications of the quantum EIT effect are considerably limited by the rigorous conditions such as stable gas lasers and low-temperature environments [5]. In addition, the EIT effect is originally observed in atomic vapors; however, the complexity of constructing atomic systems and the narrowness of the EIT window severely restrict the practical use of the EIT effect [6, 7].

Plasmon induced transparency (PIT), which is a plasmonic analogue of classical EIT, has attracted enormous attention because of its potentially important applications in the fields of integrated photonic devices and ultrahigh-speed information processing chips. It would be greatly advantageous to extend the concept of the EIT effect to the PIT effect, which is a strong destructive interference coupling between two cavities in the PIT system [8]. The principal characteristics of the PIT effect lie in the appearance of a sharp and narrow transparency window within absorption band, along with extraordinarily steep dispersion and dramatic reduction in group velocity [9]. Because of the large local electromagnetic field enhancement effect and overcoming of classical diffraction limit provided by the surface plasmon polaritons (SPPs), the plasmonic devices based on the PIT effect can be realized with small footprint. Various configurations have been proposed to date to demonstrate the PIT effects in plasmonic nanostructures, such as metamaterials [10-14], plasmonic waveguide side coupled cavities [15-17], graphene arrays structures [18-21], metallic photonic crystals [22, 23], metallic bar gratings [24], metallic nanowire grating coupled dielectric waveguide [22], and hybrid nanostructures [23, 25]. Among those reported configurations, the plasmonic waveguide side coupled cavities are of special interest for the PIT effect. The reason is that the plasmonic waveguide side coupled cavities are benefit for on-chip PIT, i.e., where the PIT effect is excited by signal light that is incident in the direction parallel to the chip surface.

Many integrated photonic devices require dynamically tunable PIT, i.e., the central wavelength and the magnitude of the PIT window varying with external parameters. The traditional and fundamental realization method is to directly adjust structural parameters of plasmonic nanostructures, e.g., cavity-cavity coupling distance, the size of the cavity, and metallic damping factor [26]. Yang et al. reported on-chip tunable PIT effect in a plasmonic waveguide side-coupled four different plasmonic comb line cavities which were covered with a 100 nm-thick poly (methyl methacrylate) (PMMA) layer [27]. A 45 nm shift in the central wavelength of the PIT window could be obtained by using the thermo-optic effect of the PMMA. Notably, the response time of the PMMA reaches the microsecond order. Therefore, an ultrafast response time of

subpicoseconds or even femtoseconds level is obtained by using the third-order nonlinear optical Kerr effect. Lu et al. reported that an optical Kerr nonlinear material of Ag-BaO was adopted to demonstrate a novel ultrafast all-optical switching [28]. But the third-order nonlinear susceptibility of Ag-BaO at the wavelength of 820 nm is too small ($\chi^{(3)} = 4.8\times10^{-10}$ esu) [28]. The pump light intensity is up to 650 MW/cm^2. Furthermore, Pu et al. have made plasmonic resonator and metal-dielectric-metal (MDM) waveguide filled with nonlinear optical Kerr medium MEH-PPV (poly(2-methoxy-5-(28-ethylhexyloxy)-PPV)) [29]. However, the operating threshold pump light intensity is currently up to 1 GW/cm^2 order because of the relatively small third-order nonlinear susceptibility of MEH-PPV. Similarly, Chai et al. realized an all-optical tunable PIT effect in a plasmonic nanostructure consisting of a gold nanowire grating in a polycrystalline lithium niobate ($LiNbO_3$) layer [22]. However, the size of polycrystalline $LiNbO_3$ grain is large and the third-order nonlinear susceptibility of polycrystalline $LiNbO_3$ film is also small ($\chi^{(3)} = 1.7\times10^{-7}$ esu). Hence, it is a considerable challenge to achieve low-power, ultrafast and dynamic tunable PIT effect in plasmonic circuits. In contrast to traditional nonlinear optical Kerr medium, graphene has a large effective third-order nonlinear susceptibility $\chi^{(3)}$ in the visible and near-infrared range, which has been confirmed by four wave mixing and Z-scan experiments [30, 31]. Such a unique property has made graphene an excellent nonlinear optical material in developing various tunable nanophotonic devices [32].

Different from the above studies, we in this paper propose an ultrafast and low-power all-optical tunable PIT in dual ring cavities side-coupled with a MDM plasmonic waveguide system. The ring cavity is used instead of the stub cavity that has already been reported in Ref. 15. The direct coupling between two ring cavities is neglected. The indirect coupling between two ring cavities is adopted in this work. By adopting the phase coupling scheme (indirect coupling) instead of the near-field coupling scheme (direct coupling), the tunability characteristic of PIT effect is more obvious. In addition, it may find applications in all-optical logic gates and optical modulation/switching based on tunable PIT effect.

To dynamically tune the PIT effect and enhance the third-order optical Kerr nonlinearity effect, the plasmonic waveguide based on graphene-Ag composite material structures is used with the footprint of <1 μm^2. A pump light at a wavelength of 830 nm is adopted [15]. Graphene has a large Kerr nonlinear coefficient of $n_2=-1.2\times10^{-7}$ cm^2/W in the visible and near-infrared range [30, 31]. The ultrafast response time of the order of 1 ps of graphene has been experimentally confirmed by Nikolaenko et al. [33]. When the pump light intensity was 5.83 MW/cm^2, π-phase shift of the transmission spectrum was achieved in two ring cavities side-coupled to a plasmonic waveguide system. The pump light intensity is reduced by adopting graphene-Ag composite material structures. With dynamically tuning the propagation phase of the plasmonic waveguide, the tunable bandwidth of about 12 nm was obtained. Moreover, the group delay of the PIT system was controlled between 0.19 and 0.68 ps. A temporal coupled mode theory is established to study the PIT effect in the plasmonic ring waveguide. The theoretical results agree well with the finite difference time domain (FDTD) simulations. The proposed PIT system can be found important potential applications in highly integrated optical circuits and networks, especially for optical modulator, light storage, ultrafast optical switching, wavelength-selective and nonlinear devices [34]. The problems on high power consumption, slow speed and untunable method in nanostructure integration photonic devices can be solved, which shows a new direction in obtaining low power consumption, ultrafast speed and dynamic tuning of optical pulse trapping of integration plasmonic nanostructures and all-optical dynamical storage of light devices in optical communication and quantum information processing. This work not only paves the way for the theoretical research of integrated photonic devices and quantum solid chips, but also provides a superior platform for the fundamental study of both nonlinear optics and quantum optics.

The rest of this paper is organized as follows: Section 2 gives the simplified system model to realize the PIT effect and analyzes the related theory; Section 3 demonstrates the PIT response by dynamically tuning the propagation phase of the plasmonic waveguide; and conclusions are given on Section 4.

2. PIT system model design and theoretical analysis

2.1. PIT system model design and theoretical model

The PIT system (Fig. 1) consists of a MDM waveguide with two asymmetrically side-coupled ring cavities. In our PIT systems, the metal cladding is assumed as Ag and the insulator is set as air and graphene. The plasmonic waveguide based on graphene-Ag composite material structures is used. The main structure parameters are the width of the plasmonic waveguide (w), the external radius of the ring cavities (R_1 and R'_1), the internal radius of the ring cavities (R_2 and R'_2), and the coupling distance between the two ring cavities (L). d_i and g_i represent the diameter and aperture-coupled length of ring cavity i (i=1, 2), respectively. Two ring cavities are installed on both sides of the plasmonic waveguide based on graphene-Ag composite material structures, as shown in Fig. 1. When transverse-magnetic (TM)-polarized lights are injected and coupled into the plasmonic waveguide, the SPPs wave is formed on the metallic interfaces and is confined in the plasmonic waveguide [15]. When the SPPs wave passes through the ring cavity, the energy can be coupled into the ring cavity. Samples of the U-shaped plasmonic waveguide (Fig. 1), which is connected by two ring cavities on both sides, are used. The U-shaped plasmonic waveguide was obtained experimentally on a silicon dioxide substrate from [35].

The Kerr nonlinear material is chosen as graphene in our study. Graphene films were grown on copper

substrates by chemical vapor deposition (CVD) using methane from Ref. [35]. The dry transfer technique can be used to transfer graphene films onto the entire PIT system. First, relatively thick poly (methy1 methacrylate) (PMMA) was coated on a graphene/copper foil. A polydimethylsiloxane (PDMS) block with a through hole in the center is attached to the PMMA/graphene/copper films by natural adhesion. The copper is then etched while the PDMS/PMMA/graphene block is floated over the solution. Using the PDMS "handle", the composite is easily rinsed and dried after etching, thereby removing the liquid used in the etching process. Next, the PDMS/PMMA/graphene composite is placed onto the target substrate, covering the entire PIT system. The substrate is heated. The heat treatment allows the wavy and rough PMMA/graphene film to make full contact with the target substrate. After heating, the adhesion of the graphene to the substrate is strong enough to peel off the PDMS block without delaminating the PMMA/graphene film. Finally, the PMMA is thermally removed in a furnace, without the use of any solvent. The graphene film was transferred onto the entire PIT system. At this time, the graphene film was covered on the entire PIT system. The graphene film that was covered on other areas except the areas of the MDM plasmonic waveguide between two nanoring resonators was etched by adopting Inductively Coupled Plasma (ICP) etching process [35]. Hence, the graphene film was covered on the MDM plasmonic waveguide between two nanoring resonators, as shown in Fig. 1.

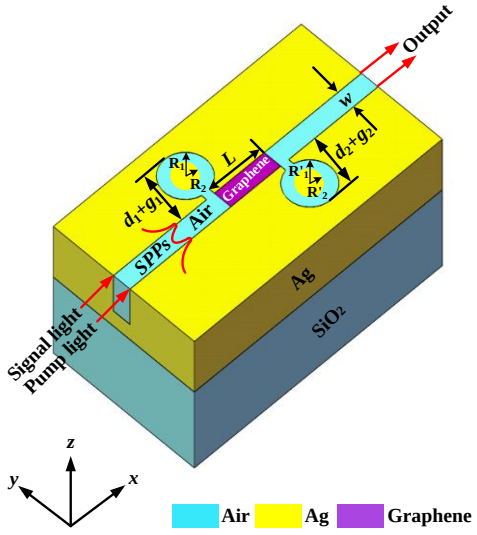

Fig. 1. Schematic of two ring cavities side-coupled to a plasmonic waveguide system, with the phase detuning between two ring cavities. The purple area indicates the Kerr nonlinear material graphene

Similar to atomic systems, wherein the interference is driven by a coherent laser field, the PIT effect could be remarkably observed through plasmonic waveguide side coupled cavities structures. The schematic of the simplified model to realize the PIT effect by two ring resonators side-coupled to a plasmonic waveguide system is shown in Fig. 2.

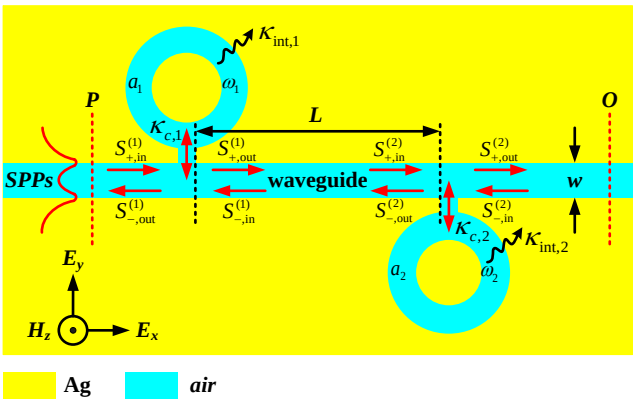

Fig. 2. Schematic of the simplified system model to realize the PIT effect

Based on the phase difference and hybridization between resonant modes of the two ring cavities, the dynamic transmission characteristics of the plasmonic structure can be analyzed by the temporal coupled mode theory. $S_{p,in}^{(i)}$ and $S_{p,out}^{(i)}$ (i=1, 2) stand for the incoming and outgoing waves in the bus waveguide. The subscript p=± represents two propagating directions of waveguide modes, as shown in Fig. 2. For the harmonic time dependence of $e^{-j\omega t}$, the dynamic equations for the cavity mode amplitudes a_i of the ith cavity can be expressed as [4]

$$\frac{da_1}{dt}=\left(-j\omega_1-\kappa_{\text{int},1}-\kappa_{c,1}\right)a_1+e^{j\theta_1}\sqrt{\kappa_{c,1}}S_{+,\text{in}}^{(1)}+e^{j\theta_1}\sqrt{\kappa_{c,1}}S_{-,\text{in}}^{(1)}, \tag{1}$$

$$\frac{da_2}{dt}=\left(-j\omega_2-\kappa_{\text{int},2}-\kappa_{c,2}\right)a_2+e^{j\theta_2}\sqrt{\kappa_{c,2}}S_{+,\text{in}}^{(2)}+e^{j\theta_2}\sqrt{\kappa_{c,2}}S_{-,\text{in}}^{(2)}, \tag{2}$$

where ω_i (i=1, 2) is the resonant frequency of the ith ring cavity, $\kappa_{int,\,i}=1/\tau_{int,\,i}=\omega_i/(2Q_{int,\,i})$ is the decay rate due to the intrinsic loss in the ith ring cavity, and $\kappa_{c,\,i}=1/\tau_{c,\,i}=\omega_i/(2Q_{c,\,i})$ is the decay rate due to energy escaping into the bus waveguide. $Q_{int,\,i}$ and $Q_{c,\,i}$ are cavity quality factors related to the intrinsic loss and the waveguide coupling loss, respectively. θ_i is the phase of the coupling coefficient. With the conservation of energy, we can get

$$S_{+,\text{out}}^{(1)}=S_{+,\text{in}}^{(1)}-e^{-j\theta_1}\sqrt{\kappa_{c,1}}a_1, \tag{3}$$

$$S_{-,\text{out}}^{(1)}=S_{-,\text{in}}^{(1)}-e^{-j\theta_1}\sqrt{\kappa_{c,1}}a_1, \tag{4}$$

$$S_{+,\text{out}}^{(2)}=S_{+,\text{in}}^{(2)}-e^{-j\theta_2}\sqrt{\kappa_{c,2}}a_2, \tag{5}$$

$$S_{-,\text{out}}^{(2)}=S_{-,\text{in}}^{(2)}-e^{-j\theta_2}\sqrt{\kappa_{c,2}}a_2, \tag{6}$$

In the linear system, since the frequency of the input

wave is ω, the field everywhere oscillates as $e^{-j\omega t}$, and $da_i/dt = -j\omega a_i$ (i=1, 2). The relationship between incoming and outgoing waves of the ith ring cavity can be expressed as

$$S_{-,\mathrm{in}}^{(1)} = \frac{\kappa_{\mathrm{c},1}}{j(\omega_1-\omega)+\kappa_{\mathrm{int},1}} S_{+,\mathrm{in}}^{(1)} + \frac{j(\omega_1-\omega)+\kappa_{\mathrm{int},1}+\kappa_{\mathrm{c},1}}{j(\omega_1-\omega)+\kappa_{\mathrm{int},1}} S_{-,\mathrm{out}}^{(1)}, \quad (7)$$

$$S_{+,\mathrm{out}}^{(1)} = \frac{j(\omega_1-\omega)+\kappa_{\mathrm{int},1}-\kappa_{\mathrm{c},1}}{j(\omega_1-\omega)+\kappa_{\mathrm{int},1}} S_{+,\mathrm{in}}^{(1)} - \frac{\kappa_{\mathrm{c},1}}{j(\omega_1-\omega)+\kappa_{\mathrm{int},1}} S_{-,\mathrm{out}}^{(1)}, \quad (8)$$

$$S_{-,\mathrm{in}}^{(2)} = \frac{\kappa_{\mathrm{c},2}}{j(\omega_2-\omega)+\kappa_{\mathrm{int},2}} S_{+,\mathrm{in}}^{(2)} + \frac{j(\omega_2-\omega)+\kappa_{\mathrm{int},2}+\kappa_{\mathrm{c},2}}{j(\omega_2-\omega)+\kappa_{\mathrm{int},2}} S_{-,\mathrm{out}}^{(2)}, \quad (9)$$

$$S_{+,\mathrm{out}}^{(2)} = \frac{j(\omega_2-\omega)+\kappa_{\mathrm{int},2}-\kappa_{\mathrm{c},2}}{j(\omega_2-\omega)+\kappa_{\mathrm{int},2}} S_{+,\mathrm{in}}^{(2)} - \frac{\kappa_{\mathrm{c},2}}{j(\omega_2-\omega)+\kappa_{\mathrm{int},2}} S_{-,\mathrm{out}}^{(2)}, \quad (10)$$

When the light is only inputted from the left port ($S_{-,\mathrm{in}}^{(2)}=0$), the transmission and reflection coefficients of single-resonator side-coupled to a plasmonic waveguide system are derived as

$$t_1(\omega) = \frac{j(\omega_1-\omega)+\kappa_{\mathrm{int},1}}{j(\omega_1-\omega)+\kappa_{\mathrm{int},1}+\kappa_{\mathrm{c},1}}, \quad (11)$$

$$t_2(\omega) = \frac{j(\omega_2-\omega)+\kappa_{\mathrm{int},2}}{j(\omega_2-\omega)+\kappa_{\mathrm{int},2}+\kappa_{\mathrm{c},2}}, \quad (12)$$

$$r_1(\omega) = -\frac{\kappa_{\mathrm{c},1}}{j(\omega_1-\omega)+\kappa_{\mathrm{int},1}+\kappa_{\mathrm{c},1}}, \quad (13)$$

$$r_2(\omega) = -\frac{\kappa_{\mathrm{c},2}}{j(\omega_2-\omega)+\kappa_{\mathrm{int},2}+\kappa_{\mathrm{c},2}}, \quad (14)$$

Therefore, incoming and outgoing waves of the ith ring cavity in two resonators side-coupled to a plasmonic waveguide system satisfy the following transfer matrix equation:

$$\begin{bmatrix} S_{-,\mathrm{in}}^{(i)} \\ S_{+,\mathrm{out}}^{(i)} \end{bmatrix} = \begin{bmatrix} -\dfrac{r_i(\omega)}{t_i(\omega)} & \dfrac{1}{t_i(\omega)} \\ 1+\dfrac{r_i(\omega)}{t_i(\omega)} & \dfrac{r_i(\omega)}{t_i(\omega)} \end{bmatrix} \begin{bmatrix} S_{+,\mathrm{in}}^{(i)} \\ S_{-,\mathrm{out}}^{(i)} \end{bmatrix}, (i=1,2). \quad (15)$$

The two ring cavities can be regarded as frequency-dependent lossy mirrors [$r_i^2(\omega)+t_i^2(\omega)<1, i=1,2$]. In the steady state, the propagation waves in the plasmonic waveguide satisfy the following equations:

$$S_{-,\mathrm{in}}^{(1)} = S_{-,\mathrm{out}}^{(2)} e^{j\phi/2}, \quad (16)$$

$$S_{+,\mathrm{in}}^{(2)} = S_{+,\mathrm{out}}^{(1)} e^{j\phi/2}, \quad (17)$$

where ϕ is the round-trip phase difference between two ring cavities. The round-trip phase difference of the system can be expressed as follows: $\phi=2m\pi+2\Delta\phi$ (where m is an integer). $\Delta\phi$ is the one-way phase shift of the system, which can be expressed as follows: $\Delta\phi=\Delta\phi_1+\Delta\phi_2$. Here, $\Delta\phi_1$ and $\Delta\phi_2$ denote the cavity-cavity phase differences due to the waveguide dispersion for the plasmonic waveguide under static condition and the optical Kerr effect modulation in graphene-Ag composite material area under dynamic condition, respectively. If the round-trip phase difference of the system is $2m\pi$, the amplitudes will be the same. Therefore, only $\Delta\phi$ is considered in calculating the system round-trip phase difference. A narrow and symmetrical PIT peak is exhibited in the transmission spectrum when the system round-trip phase difference is close to $2m\pi$. However, an asymmetrical PIT peak is generated when the system round-trip phase difference is tuned away from $2m\pi$ [15, 36].

For simplicity, we assume that there is only one input light ($S_{-,\mathrm{in}}^{(2)}=0$) in the PIT system and two ring cavities are set as the same optical loss, which means $\kappa_{c,1}=\kappa_{c,2}=\kappa$. The phase of the coupling coefficient is assumed as 0, which means $\theta_1=\theta_2=0$. For two ring resonators side-coupled to a plasmonic waveguide system, the output transmission efficiency can be derived as

$$T = |t|^2 = \left|\frac{S_{+,\mathrm{out}}^{(2)}}{S_{+,\mathrm{in}}^{(1)}}\right|^2 = \left|\frac{t_1(\omega)t_2(\omega)}{1-r_1(\omega)r_2(\omega)e^{j\phi}}\right|^2, \quad (18)$$

The effective phase shift of the transmission spectrum $\varphi(\omega)$ and the group delay τ_g, can be calculated as $\varphi(\omega)=\arg(t)$ and $\tau_g=\partial\varphi(\omega)/\partial\omega$ [4, 15, 34].

2.2. Waveguide dispersion for the plasmonic waveguide

In the static state, because of the plasmonic waveguide dispersion, the cavity-cavity phase difference $\Delta\phi_1$ for the plasmonic waveguide can be expressed as [4, 15]

$$\Delta\phi_1 = \frac{\omega_s \,\mathrm{Re}(n_{eff})L}{c}, \quad (19)$$

where ω_s is the input frequency of the signal light; L approximates to the distance between two ring cavities; c is the speed of light in free space; and n_{eff} is the effective refractive index which can be obtained by solving the dispersion equation

$$\varepsilon_m\sqrt{n_{eff}^2-\varepsilon_d}\,\tanh\left(\frac{w\pi\sqrt{n_{eff}^2-\varepsilon_d}}{\lambda}\right) = -\varepsilon_d\sqrt{n_{eff}^2-\varepsilon_m}, \quad (20)$$

where ε_{m} and ε_{d} denote the dielectric constant of the metal cladding and the dielectric waveguide with a width of w=52 nm. Frequency-dependent complex relative

permittivity of Ag can be described by the well-known Drude model of $\varepsilon_m(\omega)=\varepsilon_\infty-\omega_p^2/(\omega^2+j\omega\gamma)$ [4, 37, 38]. Here, ε_∞ is the dielectric constant at the infinite frequency; and γ and ω_p are the electron collision frequency and the bulk plasma frequency, respectively. The increased loss of Ag in the PIT nanostructure is neglected [37]. These parameters for Ag can be set as ε_∞=3.7, ω_p=9.1 eV, and γ=0.018 eV [38]. Because the dielectric is set as air, the dielectric constant of air is 1 (ε_d=1). The real part of the effective refractive index is obtained by solving equation (20), as shown in Fig. 3.

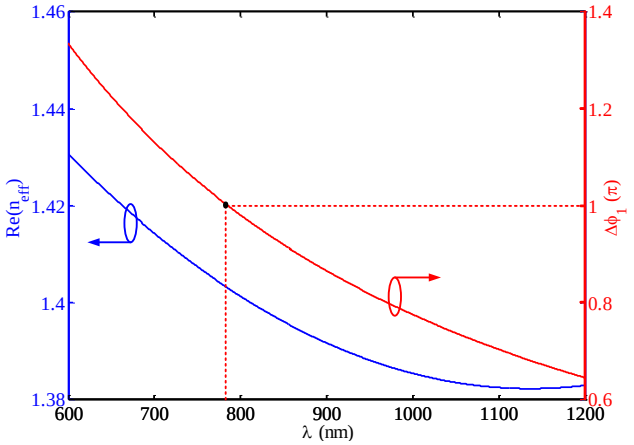

Fig. 3. Real part of the effective refractive index and phase shifts which satisfy the dispersion equation in the plasmonic waveguide with w=52 nm. The black dot represents the phase shift that satisfies the dispersion equation at λ=785 nm with value of π

Fig. 3 shows the phase shifts that satisfy the dispersion equation as a function of the wavelength. The effective refractive index is decreased due to the waveguide dispersion for the MDM plasmonic waveguide. Therefore, the phase shift is decreased with the increase in the wavelength in the MDM plasmonic waveguide with w=52 nm. In addition, the phase shift exhibits a saturated trend with the increase in the wavelength. Notably, π-phase shift is obtained in the MDM plasmonic waveguide when the wavelength increases to 785 nm. From equation (19), $\Delta\phi_1$ equals π when $\lambda=2[\mathrm{Re}(n_{eff})]L$. In Fig. 3, the optimal wavelength is 785 nm when the distance between two ring cavities is 280 nm, which agrees well with the parameter setting.

2.3. Optical Kerr effect modulation

To describe the low-power, ultrafast, and dynamic all-optical tunable PIT effect in two ring resonators side-coupled to a MDM waveguide system, the refractive index modulation method is discussed. Electrical or optical modulation methods, which are related to the thermo–effect, have been adopted in previous studies [2, 36]. However, the tuning speed of the thermo–effect is too slow. Moreover, thermo–effects resulting from nonlinear adsorption interfere with the nonlinear dynamic if not properly handled [15, 39, 40].

Nowadays, many integration photonic nonlinear devices, including all–optical switches, all–optical modulators, and all–optical memories, require ultrafast response times and low pump powers. Ultrafast response times can be attained by using an optical Kerr effect modulation method. Graphene is a monolayer of carbon atoms arranged in a hexagonal two-dimensional crystal lattice. In addition, graphene has flat linear absorption of approximately 2.3% across the entire visible and near-infrared range. Enormously enhanced optical Kerr effect can be realized in graphene because of its unique linear and massless band structure, i.e., interband optical transitions can occur at all photon energies. Therefore, graphene is an excellent nonlinear optical material with an ultrafast response time and high optical Kerr nonlinearity effect [35]. To study low-power, ultrafast, and dynamic all-optical tunable PIT effect in two ring resonators side-coupled to a MDM waveguide system, the plasmonic waveguide based on graphene-Ag composite material structures is used. A pump light at a wavelength of 830 nm is adopted in our research [15].

The optical Kerr effect is responsible for the intensity dependent refractive index n_2 and related to the real part of $\chi^{(3)}$. The refractive index of the material is linearly dependent on the optical intensity I. The Kerr-induced refractive index change of graphene is defined as $\Delta n=n_{2eff}I$, where n_{2eff} is the effective Kerr nonlinear coefficient. Graphene-Ag composite material structures have a large effective Kerr nonlinear coefficient $n_{2eff}\approx n_2=-1.2\times10^{-7}$ cm^2/W [35]. The effective refractive index n of graphene is expressed as $n=n_0+n_{2eff}I\approx n_0+n_2I$, where n_0=2.4 is the effective linear refractive index of graphene [15, 35]. In the dynamic state, because of the optical Kerr effect modulation, the change in the effective refractive index results in the effective phase change of the waveguide signal light

$$\Delta\phi_2=\frac{2\pi}{\lambda_s}\Delta n_{eff}L, \tag{21}$$

where $\Delta n_{eff}\approx\Delta n$; and λ_s is the wavelength of the signal light.

Therefore, a part of the phase difference between two ring cavities comes from the dispersion equation of the SPPs wave in the static state; the other part is from the optical Kerr effect modulation in the plasmonic waveguide based on graphene-Ag composite material structures in the dynamic state [15].

Fig. 4 shows the phase shift of the induced signal light as a function of the pump light intensity. The plot of Fig. 4 is based on equation (21). Because of the negative value of the effective Kerr nonlinear coefficient, the effective refractive index of graphene-Ag composite material structures is decreased under the pump light excitation, which leads to a blue shift in the resonant wavelength of the PIT system. The optical Kerr effect decreases the effective refractive index of the plasmonic waveguide

based on graphene-Ag composite material structures. When I >0, the phase shift of the induced signal light decreases, so $\Delta\phi_2$ <0. The phase shift of the induced signal light exhibits a linear trend with the increase of the pump light intensity because of the optical Kerr effect modulation. The phase shifts of the induced signal light are 0.5π and π when the pump light intensities are 5.83 and 11.66 MW/cm^2, respectively. The pump light intensities are reduced by adopting graphene-Ag composite material structures. The reason is that the optical Kerr effect is enhanced by the local electromagnetic field of SPPs and the plasmonic waveguide based on graphene-Ag composite material structures with large effective Kerr nonlinear coefficient [15].

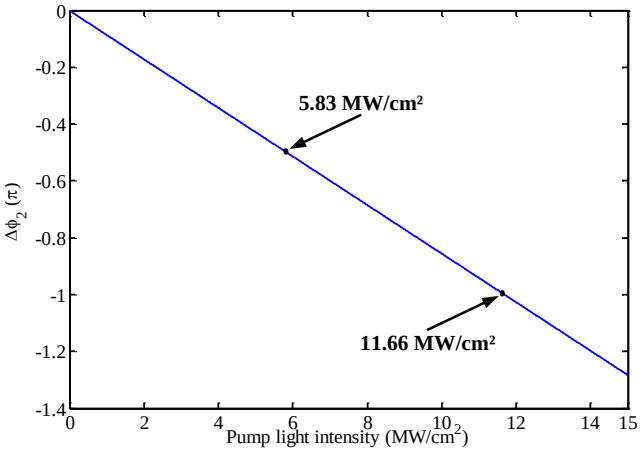

Fig. 4. Relationship between the phase shift of the induced signal light and the pump light intensity

2.4. Quality factors in the plasmonic coupled ring nanocavities

To analyze the transmission response, the phase shift of the transmission spectrum and the group delay of the PIT effect, the quality factors $Q_{\text{int},1}$, $Q_{\text{int},2}$, $Q_{\text{c},1}$, and $Q_{\text{c},2}$ should be obtained. Here, the intrinsic quality factor Q_{int} of the ring cavity can be estimated by solving the following equations [4, 41]:

$$\frac{\sqrt{\varepsilon_m}J_n'(k\sqrt{\varepsilon_d}R_{eff})}{J_n(k\sqrt{\varepsilon_d}R_{eff})}=\frac{\sqrt{\varepsilon_d}H_n^{(1)\prime}(k\sqrt{\varepsilon_m}R_{eff})}{H_n^{(1)}(k\sqrt{\varepsilon_m}R_{eff})}, \tag{22}$$

$$Q_{\text{int}}=-\frac{\text{Re}(k)}{2\,\text{Im}(k)}, \tag{23}$$

where R_{eff} denotes the effective radius of the ring cavity. k is the wave number in vacuum and includes a relatively small negative imaginary part for a given n, where the negative imaginary part presents the loss. J_n and J_n' are Bessel function of the first kind with the order n and its derivative, respectively. $H_n^{(1)}$ and $H_n^{(1)'}$ are Hankel function of the first kind with the order n and its derivative, respectively. The fundamental mode is considered in the frequency range, which corresponds to the first order (n=1) Bessel and Hankel functions [4, 41]. Q_{int} is a function of the effective radius of the ring resonator. The total quality factor Q_t of the side-coupled resonator can be obtained from $Q_t = \lambda_0/\Delta\lambda$, where λ_0 and $\Delta\lambda$ are the peak wavelength and full width at half maximum (FWHM) of the reflection spectrum, respectively. Under the condition of $Q_{\text{int}} >> Q_c$, the coupling quality factor can be obtained from the equation $Q_c = Q_{\text{int}}Q_t/(Q_{\text{int}}-Q_t)$ [4, 42].

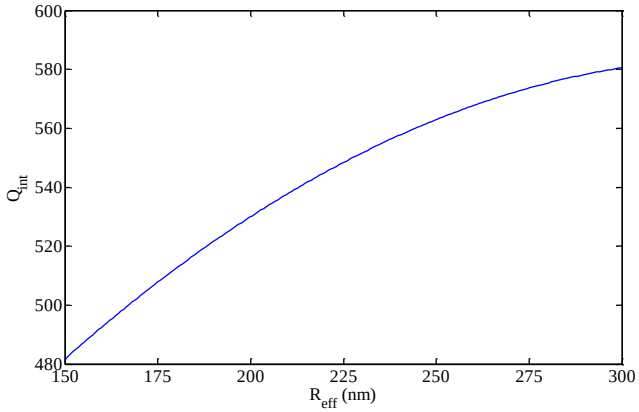

Fig. 5. Relationship between the intrinsic quality factor (Q_{int}) and the effective radius of the ring resonator

In our plasmonic system, details on the structural parameters have been given in this work. As depicted in Fig. 5, Q_{int} is about 530 when the effective radius of cavities 1 and 2 are set as 196 and 200 nm, respectively. By using FDTD simulation, Q_t is about 65. Hence, Q_c is about 74.1 for the side-coupled resonators. For FDTD simulation, the time accuracy of FDTD simulation is set as 3000 fs. Perfectly matched layer conditions are adopted to absorb output waves from the computation domain; the spatial and temporal steps are set as $\Delta x = \Delta y = 2$ nm and $\Delta t = \Delta x/2c$, respectively. The resonant wavelengths of cavities 1 and 2 are 779 and 791 nm, respectively. The transparent wavelength is 785 nm. For the waveguide dispersion in the MDM plasmonic waveguide, the wavelength is 785 nm when $\Delta\phi_1$ equals π and the distance between two ring cavities is 280 nm (Fig. 3), which agrees well with the FDTD method.

3. Propagation phase of the plasmonic waveguide tuning the PIT effect

Recently, Wang et al. reported that the PIT effect was researched in dual-stub-coupled MDM waveguide by incorporating a PMMA layer (or a monolayer graphene) with the plasmonic waveguide and using FDTD simulations [15, 43-45]. Different from [15, 44, 45], in our

proposed structure, dual-ring-coupled MDM waveguide is used by incorporating a monolayer graphene with the plasmonic waveguide. The tunable refractive index material graphene is used instead of PMMA in this paper. The reason is that graphene is an excellent nonlinear optical material with an ultrafast response time and high optical Kerr nonlinearity effect. Moreover, the ring cavity is used instead of the stub cavity in this paper. The reason is that the direct coupling between two ring cavities is neglected and the PIT effect is more obvious. In our simulations, the effective refractive index n_{eff} of graphene is related to the pump light intensity I. When the effective refractive index of graphene is fixed, the effective refractive index n_{eff} of the excited SPPs wave changes with the alteration of the incident frequency [15, 44-49]. The transmission intensity spectral responses in our PIT system for different refractive indices of graphene are researched.

Fig. 6 shows the normalized transmission intensity spectra, corresponding phase shift responses, and group delay under various pump light intensities (from 0 to 11.66 MW/cm^2) or phase differences between two ring cavities (from π to 0) in two resonators side-coupled to a plasmonic waveguide system. The transmission intensity spectral responses in the PIT system are researched by the dynamic temporal coupled mode equations and the FDTD method. The theoretical results are in good agreement with FDTD simulations. Fig. 6(a) (i) and (v) show that an symmetrical PIT transmission peak is generated. The reason is that the direct coupling between two ring cavities is not considered. Moreover, the PIT transmission intensity spectra are the same when the phase shift between two ring cavities is tuned to π. However, the phase shift of the transmission spectrum is changed 2π (from Fig. 6(b) (i)–(v)) because the optical Kerr effect results in the decrease in the effective refractive index of the plasmonic waveguide.

The PIT system round-trip phase is close to $2m\pi$ (m=0, 1), resulting in a Fabry-Perot resonance. The strong coupling interference condition between two ring cavities is satisfied. Therefore, the maximum transmission intensity of the transparent wavelength at 785 nm is obtained, which means the coherent interaction between two ring cavities is the strongest, as shown in Fig. 6(a) (i) and (v). In addition, the maximum group delay of the PIT transparency window is obtained, which means more time is spent between two ring cavities, as shown in Fig. 6(c) (i) and (v).

When $\Delta\phi \in [\pi, 0.5\pi)$, the PIT transmission window blue-shifts and the transmission intensity is reduced, as shown in Fig. 6(a) (i) and (ii). However, when $\Delta\phi \in [0.5\pi, 0)$, the PIT transmission window red-shifts and the transmission intensity is increased, as shown in Fig. 6(a) (iii) and (iv). In Fig. 6(a) (ii) and (iv), the systems round-trip phase is tuned away from $2m\pi$, resulting in an asymmetric transmission spectra and group delay spectra, which results from the dissatisfaction of the coupling interference condition between two ring cavities. However, the group delays of the transparent wavelength at 785 nm are the same, as shown in Fig. 6(c) (ii) and (iv). When $\Delta\phi = 0.5\pi$, the coupling strength between two ring cavities is at its weakest with a minimum value in the transmission spectrum (Fig. 6(a) (iii)), which results from the dissatisfaction of Fabry-Perot resonance condition of the waveguide phase. Hence, the minimum transmission intensity and the group delay of the transparent wavelength at 785 nm are obtained, as shown in Fig. 6(a) (iii) and (c) (iii). Notably, the corresponding phase shift values of the transparent wavelength at 785 nm are -2π, -1.59π, $-\pi$, -0.48π, and 0π (Fig. 6(b) (i)–(v)). The corresponding group delay values of the transparent wavelength at 785 nm are 0.68, 0.45, 0.19, 0.45, and 0.68 ps (Fig. 6(c) (i)–(v). To further clarify the physical reason for the PIT phenomenon, the field distributions of $|H_z|^2$ are calculated by using the FDTD method at the two dip wavelengths and the transmission peak wavelength, as shown in Fig. 7(a)–(c). It is found that the two ring cavities act as two resonators. The appearance of a transmission peak at 785 nm is attributed to the Fabry-Perot resonance between two ring cavities. Therefore, the incident light can propagate through the plasmonic waveguide system uninhibitedly at wavelength 785 nm, while being stored in ring cavities and reflected back at the other two wavelengths.

Fig. 8 shows the relationship between the phase shift of the waveguide signal light and the phase shift of the transmission spectrum at the transparent wavelength of 785 nm. Phase shifts of the transmission spectra are zero and $-\pi$ when phase shifts between two ring cavities $\Delta\phi$ are zero and 0.5π, respectively. Apparently, π-phase shift and 2π-phase shift of the transmission spectrum are obtained when the propagation phase of the plasmonic waveguide is tuned to 0.5π-phase shift and π-phase shift, respectively, as shown in Fig. 8. Therefore, the phase shift multiplication effect of the PIT effect is found. When $\Delta\phi = 0.5\pi$, the weak coupling interference condition between two ring cavities is satisfied. The coupling strength between two ring cavities is at its weakest. In this case, the two ring cavities can only interact with each other indirectly. The PIT effect can be realized by the indirect coupling or the phase coupling scheme. The phase shift multiplication effect of the PIT effect is not influenced by the direct coupling between two ring cavities under both the weak and the strong coupling interference conditions. The reason is that the direct coupling between two ring cavities is not considered in our PIT system.

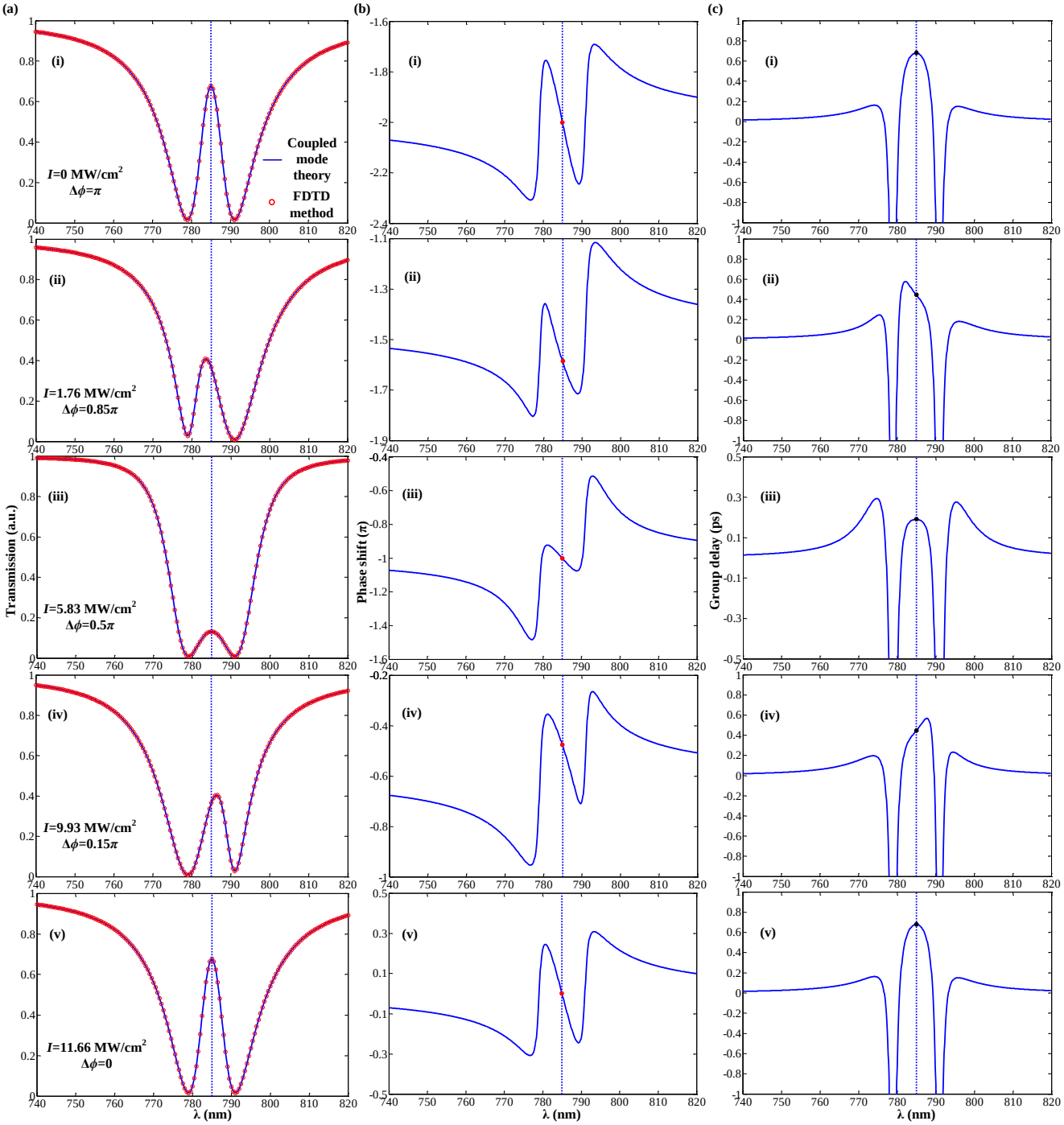

Fig. 6. Normalized transmission intensity spectra, corresponding phase shift responses, and group delay under different pump light intensities in two resonators side-coupled to a waveguide system. a(i)−(v) PIT transmission intensity spectra. b(i)–(v) Corresponding phase shift responses. The red dots represent the corresponding phase shifts of the transparent wavelength at 785 nm with values of −2π, −1.59π, −π, −0.48π, and 0π. c(i)–(v) Group delay. The black dots represent the group delays of the transparent wavelength at 785 nm with values of 0.68, 0.45, 0.19, 0.45, and 0.68 ps

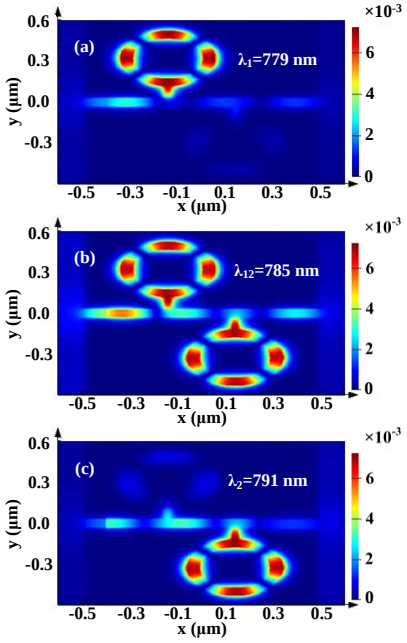

Fig. 7. Field distributions of $|H_z|^2$ at the transmission dip wavelength of 779 nm (a) and 791 nm (c) and the transparent wavelength of 785 nm (b) when the pump light intensity is 11.66 MW/cm^2. The corresponding transmission spectrum is shown in Fig. 6(a)(v)

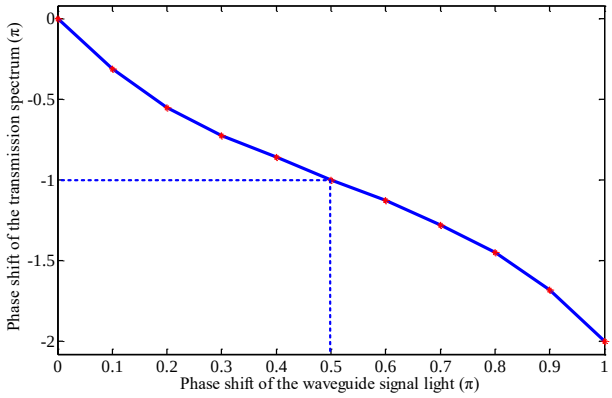

Fig. 8. Phase shifts of the transmission spectrum at the transparent wavelength of 785 nm as a function of phase shifts of the waveguide signal light

Similar to the EIT effect in the atomic system, the PIT system also supports slow group velocities. The slow light effect can be described by the group index n_g, which is expressed as [4, 15]

$$n_g = \frac{c}{v_g} = \frac{c}{l}\tau_g = \frac{c}{l}\cdot\frac{\partial\varphi(\omega)}{\partial\omega}. \quad (24)$$

Here, v_g stands for the group velocity in the PIT system. l is the length of the plasmonic system. The slow light behavior is numerically investigated in the PIT system with L=280 nm and l=1 μm.

In the PIT system, the group delay is controlled between 0.19 and 0.68 ps by dynamically tuning the propagation phase of the plasmonic waveguide, as shown in Table 1. The group delay of the PIT transparency peak decreases with the increase in pump light intensities but increases when the system round-trip phase is π, indicating that the group delay of the PIT system is influenced by the coupling interference strength between two ring cavities. When $\Delta\phi = 0.5\pi$, the weak coupling interference condition between two ring cavities is satisfied. The minimum group delay of 0.19 ps at the PIT transparency peak is obtained. Hence, very little coherent interaction exists between two ring cavities, and the group delay of the system is mainly caused by the direct-path delay. However, when $\Delta\phi = m\pi$ (m = 0, 1), the strong coupling interference condition between two ring cavities is satisfied. The maximum group delay of 0.68 ps at the PIT transparency peak is obtained. High group indices around the transparency peak result from the strong dispersion in the transparency window. The coherent interaction between two ring cavities is the strongest, which means more time is spent between two ring cavities.

Table 1. Phase shifts between two cavities, effective phase shifts and corresponding group delays of the PIT transmission spectra at a transparent wavelength of 785 nm under different pump light intensities in two ring cavities side-coupled with a waveguide system

Pump light intensities, I (MW/cm^2)	Phase shifts between two cavities, $\Delta\phi$ (π)	Effective phase shifts of the transparent wavelength at 785 nm, φ (π)	Group delays of the transparent wavelength at 785 nm, τ_g (ps)
0	1	−2	0.68
1.76	0.85	−1.59	0.45
5.83	0.5	−1	0.19
9.93	0.15	−0.48	0.45
11.66	0	0	0.68

4. Conclusions

In conclusion, an ultrafast and low-power all-optical tunable PIT in dual ring cavities side-coupled with a MDM plasmonic waveguide system with nonlinear optical Kerr medium is investigated both theoretically and numerically. The response time of optical Kerr effect modulation method was applied to improve the tuning rate because it has a response time of subpicoseconds or even femtoseconds. The phase coupling scheme is adopted. With dynamically tuning the propagation phase of the plasmonic waveguide, π-phase shift of the transmission spectrum in the PIT system is achieved under excitation of a pump light with an intensity as low as 5.83 MW/cm^2. The pump light intensity is reduced by adopting graphene-Ag composite material structures. The reason is that the optical Kerr effect is enhanced by the slow light effect of the PIT effect, the local electromagnetic field of SPPs and the plasmonic waveguide based on graphene-Ag composite material structures with large effective Kerr nonlinear coefficient. The tunable wavelength range of the transparency window center reached about 12 nm. The phase shift multiplication effect of the PIT effect is not influenced by the direct coupling between two ring cavities under both the weak and the strong coupling interference conditions. The results may open up avenues for designing nanoscale ultrasensitive sensors, ultrafast optical switching, ultrafast phase modulators, and light storage in highly integrated optical circuits.

Acknowledgments

This work is supported by the National Natural Science Foundation of China (Grant Nos 11647122 and 61705064), the Natural Science Foundation of Hubei Provincial (Grant Nos 2018CFB672 and 2018CFB773), and the Research Foundation of Education Bureau of Hubei Province, China (Grant No. T201617).

References

[1] S. E. Harris, Phys. Today **50** (7), 36 (1997).
[2] X. Yang, M. Yu, D.-L. Kwong, C. W. Wong, IEEE J. Sel. Top. Quantum Electron. **16** (1), 288 (2010).
[3] W. B. Robert, J. G. Daniel, Nature **441**(7094), 701 (2006).
[4] H. Lu, X. Liu, D. Mao, Phys. Rev. A **85** (5), 053803 (2012).
[5] R. D. Kekatpure, E. S. Barnard, W. Cai, M. L. Brongersma, Phys. Rev. Lett. **104** (24), 243902 (2010).
[6] L. Zhou, T. Ye, J. Chen, Opt. Lett. **36**(1), 13 (2011).
[7] Z. Zou, L. Zhou, X. Sun, J. Xie, H. Zhu, L. Lu, X. Li, J. Chen, Opt. Lett. **38**(8), 1215 (2013).
[8] S. Zhang, D. A. Genov, Y. Wang, M. Liu, X. Zhang, Phys. Rev. Lett. **101**(4), 047401 (2008).
[9] T. Wang, Y. S. Zhang, Z. Hong, Z. H. Han, Opt. Express **22**(18), 21529 (2014).
[10] S. Xiao, T. Wang, X. Jiang, X. Yan, L. Cheng, B. Wang, C. Xu, Journal of Phys. D: Appl. Phys. **50**(19), 195101 (2017).
[11] S. Xiao, T. Wang, Y. Liu, X. Han, X. Yan, Plasmonics **12**(1), 185 (2017).
[12] S. Xiao, T. Wang, T. Liu, X. Yan, Z. Li, C. Xu, Carbon **126**, 271 (2018).
[13] J. Gu, R. Singh, X. Liu, X. Zhang, Y. Ma, S. Zhang, S. A. Maier, Z. Tian, A. K. Azad, H.-T. Chen, A. J. Taylor, J. Han, W. Zhang, Nature Commun. **3**(1151), 1 (2012).
[14] Y. Ling, L. Huang, W. Hong, T. Liu, J. Luan, W. Liu, J. Lai, H. Li, Nanoscale **10**(41), 19517 (2018).
[15] B. Wang, Q. Zeng, S. Xiao, C. Xu, L. Xiong, H. Lv, J. Du, H. Yu, Journal of Phys. D: Appl. Phys. **50**(45), 455107 (2017).
[16] X. Han, T. Wang, X. Li, B. Liu, Y. He, J. Tang, Journal of Lightwave Technology **33**(14), 3083 (2015).
[17] G. T. Cao, H. J. Li, S. P. Zhan, H. Q. Xu, Z. M. Liu, Z. H. He, Y. Wang, Opt. Express **21**(8), 9198 (2013).
[18] S. Xiao, T. Wang, X. Jiang, B. Wang, C. Xu, Plasmonics **13**(3), 185 (2018).
[19] S. Xiao, T. Wang, Y. Liu, C. Xu, X. Han, X. Yan, Phys. Chem. Chem. Phys. **18**(38), 26661 (2016).
[20] X. Jiang, T. Wang, S. Xiao, X. Yan, L. Cheng, Opt. Express **25**(22), 27028 (2017).
[21] S. Yan, X. Zhu, L. H. Frandsen, S. Xiao, N. A. Mortensen, J. Dong, Y. Ding, Nature Commun. **8**, 14411 (2017).
[22] Z. Chai, X. Y. Hu, Y. Zhu, F. Zhang, H. Yang, Q. H. Gong, Appl. Phys. Lett. **102**(20), 201119 (2013).
[23] T. Utikal, T. Zentgraf, T. Paul, C. Rockstuhl, F. Lederer, M. Lippitz, H. Giessen, Phys. Rev. Lett. **106**(13), 133901 (2011).
[24] Z. G. Dong, P. G. Ni, J. Zhu, X. Zhang, Opt. Express **20**(7), 7206 (2012).
[25] Z. R. Zhang, L. W. Zhang, H. Q. Li, H. Chen, Appl. Phys. Lett. **104**(23), 231114 (2014).
[26] X. Han, T. Wang, B. Wang, B. Liu, Y. He, Y. Zhu, J. Appl. Phys. **117**(10), 103105 (2015).
[27] X. Y. Yang, X. Y. Hu, Z. Chai, C. C. Lu, H. Yang, Q. H. Gong, Appl. Phys. Lett. **104**(22), 221114 (2014).
[28] H. Lu, X. Liu, L. Wang, Y. Gong, D. Mao, Opt. Express **19**(4), 2910 (2011).
[29] M. Pu, N. Yao, C. Hu, X. Xin, Z. Zhao, C. Wang, X. Luo, Opt. Express **18**(20), 21030 (2010).
[30] E. Hendry, P. J. Hale, J. Moger, A. K. Savchenko, Phys. Rev. Lett. **105**(9), 097401 (2010).
[31] H. Zhang, S. Virally, Q. L. Bao, L. K. Ping, S. Massar, N. Godbout, P. Kockaert, Opt. Lett. **37**(11), 1856 (2012).
[32] X. Han, T. Wang, X. Li, S. Xiao, Y. Zhu, Opt. Express **23**(25), 31945 (2015).
[33] A. E. Nikolaenko, N. Papasimakis, E. Atmatzakis, Z. Luo, Z. X. Shen, F. D. Angelis, S. A. Boden, E. D. Fabrizio, N. I. Zheludev, Appl. Phys. Lett. **100**(18), 181109 (2012).

[34] B. Wang, T. Wang, X. Li, X. Han, Y. Zhu, J. Appl. Phys. **117**(21), 213106 (2015).
[35] Y. Zhu, X. Y. Hu, H. Yang, Q. H. Gong, Sci. Rep. **4**, 3752 (2014).
[36] X. Yang, M. Yu, D.-L. Kwong, C. W. Wong, Phys. Rev. Lett. **102**(17), 173902 (2009).
[37] J. Park, H. Kim, B. Lee, Opt. Express **16**(1), 413 (2008).
[38] Z. H. Han, S. I. Bozhevolnyi, Opt. Express **19**(4), 3251 (2011).
[39] S. Combrie, Q. V. Tran, A. D. Rossi, C. Husko, P. Colman, Appl. Phys. Lett. **95**(22), 221108 (2009).
[40] A. D. Rossi, M. Lauritano, S. Combrie, Q. V. Tran, C. Husko, Phys. Rev. A **79**(4), 043818 (2009).
[41] C. Ioannis, J. Opt. Soc. Am. A **26**(12), 2623 (2009).
[42] S. Zhan, H. Li, G. Cao, Z. He, B. Li, H. Yang, Journal of Phys. D: Appl. Phys. **47**(20), 205101 (2014).
[43] G. Wang, H. Lu, X. Liu, Opt. Express **20**(19), 20902 (2012).
[44] G. Wang, W. Zhang, Y. Gong, J. Liang, IEEE Photonics Technol. Lett. **27**(1), 89 (2015).
[45] G. Wang, H. Lu, X. Liu, Appl. Phys. Lett. **101**(1), 013111 (2012).
[46] Z. Yi, C. Liang, X. Chen, Z. Zhou, Y. Tang, X. Ye, Y. Yi, J. Wang, P. Wu, Micromachines **10**(7), 443 (2019).
[47] C. Cen, Z. Yi, G. Zhang, Y. Zhang, C. Liang, X. Chen, Y. Tang, X. Ye, Y. Yi, J. Wang, J. Hua, Results in Phys. **14**, 102463 (2019).
[48] Z. Yi, J. Huang, C. Cen, X. Chen, Z. Zhou, Y. Tang, B. Wang, Y. Yi, J. Wang, P. Wu, Results in Phys. **14**, 102367 (2019).
[49] Y. Zhang, C. Cen, C. Liang, Z. Yi, X. Chen, M. Li, Z. Zhou, Y. Tang, Y. Yi, G. Zhang, Results in Phys. **14**, 102422 (2019).

*Corresponding author: d201277589@alumni.hust.edu.cn; yuhuaqing@126.com